Ivchenko, V.O.; Sinha, B.; Zalesny, V.B.; Marsh, R.; Blaker, A.T.. 2013 Influence of bottom topography on integral constraints in zonal flows with parameterized potential vorticity fluxes. *Journal of Physical Oceanography*, 43 (2). 311-323. 10.1175/JPO-D-12-0126.1

Influence of Bottom Topography on Integral Constraints in Zonal Flows with Parameterized Potential Vorticity Fluxes

V. O. IVCHENKO

University of Southampton, National Oceanography Centre, Southampton, United Kingdom

B. SINHA

National Oceanography Centre, Southampton, United Kingdom

V. B. ZALESNY

Institute of Numerical Mathematics, Moscow, Russia

R. MARSH

University of Southampton, National Oceanography Centre, Southampton, United Kingdom

A. T. BLAKER

National Oceanography Centre, Southampton, United Kingdom

(Manuscript received 17 June 2012, in final form 10 October 2012)

ABSTRACT

An integral constraint for eddy fluxes of potential vorticity (PV), corresponding to global momentum conservation, is applied to two-layer zonal quasigeostrophic channel flow. This constraint must be satisfied for any type of parameterization of eddy PV fluxes. Bottom topography strongly influences the integral constraint compared to a flat bottom channel. An analytical solution for the mean flow solution has been found by using asymptotic expansion in a small parameter, which is the ratio of the Rossby radius to the meridional extent of the channel. Applying the integral constraint to this solution, one can find restrictions for eddy PV transfer coefficients that relate the eddy fluxes of PV to the mean flow. These restrictions strongly deviate from restrictions for the channel with flat bottom topography.

1. Introduction

Mesoscale variability in the ocean produces a strong maximum in the kinetic energy spectrum. The horizontal scale of such motion is usually comparable with Rossby radius of deformation and is small relative to the size of ocean basins (Kamenkovich et al. 1986).

Mesoscale eddies can substantially affect the large-scale ocean circulation. In some circumstances eddies can transfer their energy to the large-scale flow (Scott and Wang 2005), and in others they take energy from the large scale circulation (Kamenkovich et al. 1986). In zonal flows mesoscale eddies can influence the large-scale flow (McWilliams et al. 1978; McWilliams and Chow 1981; Treguier and McWilliams 1990; Wolff et al. 1991; Ivchenko et al. 1997). Eddies can both decrease mean momentum and concentrate momentum in the center of jets.

Eddy-resolving numerical ocean circulation models, which allow development of mesoscale eddies, being averaged in space and time produce different time- and space-averaged solutions compared with coarse-resolution models without parameterization of eddies. In spite of enormous improvements in computer hardware and software, numerical simulations for climatological purposes (many decades) with very high resolution remain unrealistic. Therefore parameterization of mesoscale eddies is an important problem in modern oceanography.

Averaging over the system of dynamical equations introduces eddy fluxes of momentum, temperature, salinity,

Corresponding author address: V. O. Ivchenko, University of Southampton, National Oceanography Centre, Southampton United Kingdom.
E-mail: voi@noc.soton.ac.uk

DOI: 10.1175/JPO-D-12-0126.1

potential vorticity, and the other properties. The nature of these fluxes is unknown a priori. Mesoscale variability cannot be ignored and we have to either describe (resolve) individual eddies, or parameterize them, that is, develop physically correct links between eddy fluxes and mean variables and their gradients.

There has been substantial interest in diffusive parameterizations of eddy fluxes of potential vorticity, which introduce transfer coefficients in recent studies (Eden 2010; Eden and Greatbatch 2008; Marshall et al. 2012; Marshall and Adcroft 2010; Ringler and Gent 2011).

The important step that should be considered before using any parameterization scheme is to formulate integral constraints. In the basic equations the eddy fluxes arising after averaging from the nonlinear advection terms and therefore can be written in divergent form (divergence of eddy fluxes). If these equations are integrated over the whole basin the divergence of eddy fluxes results in normal fluxes through the lateral boundaries and the sea floor (with variable bottom topography). The normal fluxes either cancel or must be balanced by other processes. This requirement, which is an integral constraint on the flow, must be satisfied for any type of parameterization. This leads to restrictions on the transfer coefficients, introduced by the specific type of parameterization.

The simplest example of an integral constraint can be shown for quasigeostrophic zonal flow. The well-known Bretherton theorem (Bretherton 1966) states that the integral of meridional eddy flux of potential vorticity must be zero for a flat bottom zonal channel. This theorem means conservation of total mean zonal flow: eddies only redistribute zonal momentum (see section 2). The momentum input to the zonal channel is balanced by viscous bottom friction and partly by viscous lateral friction in the flat bottom domain. Applying this constraint to a diffusive parameterization of potential vorticity, Marshall (1981) demonstrated that the transfer coefficient in the lower layer of a two-layer model must be higher than the coefficient in the upper layer for a flat bottom channel. He showed that this feature of the transfer coefficients of potential vorticity (CPV) is linked with Pedlosky's instability conditions (Pedlosky 1979).

What happens in a similar zonal channel but with bottom topography? In this case the input by wind is balanced mainly by inviscid topographic form stress (Munk and Palmén 1951; Ivchenko et al. 1996; Stevens and Ivchenko 1997) but not viscous terms. This means that the integral constraint is severely distorted compared to the Bretherton theorem. Indeed, the total eddy flux of PV is not zero, but equal to the integrated topographic form stress (Ivchenko 1987; Vallis 2006). How this modified constraint influences the effective values of the transfer coefficients for a diffusive parameterization is the main object of this study.

This study combines two different approaches:

(i) the numerical eddy-resolving experiment (Section 3, and Figs. 1–7); and
(ii) application of an analytical solution for the steady-state quasigeostrophic channel model with topography (sections 4 and 5) to the integral constraint (section 6 and Figs. 8 and 9).

Using the numerical model allows us to see the solution with explicit interaction of eddies and the mean flow, that is, without parameterization. This allows us to have a view of developing channel flow, to consider the zonally averaged profiles and amplitude spectrum of the streamfunction.

The analytical solution represents a major part of the study. We use parameters taken directly from the numerical results in our analytical solution.

2. Basic quasigeostrophic equation for the zonal channel

The quasigeostrophic equations for the two-layer model can be written as

$$\frac{\partial q_1}{\partial t} + J(\Psi_1, q_1) = 1/H_1 \mathrm{curl}_z \boldsymbol{\tau} + F_1, \quad \text{and} \tag{1}$$

$$\frac{\partial q_2}{\partial t} + J(\Psi_2, q_2) = -\epsilon \mathrm{curl}_z \mathbf{v}_2 + F_2, \tag{2}$$

where q_i and Ψ_i are quasigeostrophic potential vorticity (QPV) and streamfunction, respectively; subscripts 1 and 2 mark the upper and lower layers whose mean thicknesses H_i are constant; $\boldsymbol{\tau}$ is the wind stress. Here, $\mathbf{v}_i$ is the vector of horizontal velocity, with the zonal component $u_i = -\partial\Psi_i/\partial y$, and meridional component $v_i = -\partial\Psi_i/\partial x$; F_i is the lateral friction; and $J(\cdot,\cdot)$ is the Jacobian operator, $J(A, B) = -(\partial A/\partial y)(\partial B/\partial x) + (\partial A/\partial x)(\partial B/\partial y)$.

The layer-wise potential vorticities q_i are given by

$$q_1 = \nabla^2\Psi_1 + f - \frac{f_0^2}{g' H_1}(\Psi_1 - \Psi_2), \quad \text{and} \tag{3}$$

$$q_2 = \nabla^2\Psi_2 + f + \frac{f_0^2}{g' H_2}(\Psi_1 - \Psi_2) + \frac{f_0}{H_2} B, \tag{4}$$

where $g' = g(\rho_2 - \rho_1)/\rho_0$ is the reduced gravity, g is the acceleration due to gravity; ρ_i is the averaged density of layer i and ρ_0 is a reference density. Here, f and f_0 are the Coriolis parameter and its value at a reference latitude, respectively, and B is the deviation of bottom topography from the constant depth of $H = H_1 + H_2$.

Averaging Eqs. (1)–(4) in time and zonally results in

$$\frac{\partial \overline{q}_1}{\partial t} = -\frac{\partial}{\partial y}\overline{v_1' q_1'} - 1/H_1 \frac{\partial}{\partial y}\overline{\tau}_x + F_1, \quad (5)$$

$$\frac{\partial \overline{q}_2}{\partial t} = -\frac{\partial}{\partial y}\overline{v_2' q_2'} + \epsilon \frac{\partial}{\partial y}\overline{u_2} + F_2, \quad (6)$$

$$\overline{q}_1 = -\frac{\partial}{\partial y}\overline{u}_1 + f - \frac{f_0^2}{g' H_1}(\overline{\Psi}_1 - \overline{\Psi}_2), \quad \text{and} \quad (7)$$

$$\overline{q}_2 = -\frac{\partial}{\partial y}\overline{u}_2 + f + \frac{f_0^2}{g' H_2}(\overline{\Psi}_1 - \overline{\Psi}_2) + f_0/H_2 \overline{B}. \quad (8)$$

The overbar and prime denote the time and zonal average and the eddy component (the deviation from the zonal-time mean), respectively.

The well-known condition for conservation of momentum in a zonal flat bottom channel in the absence of external forcing and friction is the theorem of Bretherton (Bretherton 1966; McWilliams et al. 1978):

$$\int_0^L (H_1 \overline{v_1' q_1'} + H_2 \overline{v_2' q_2'})\, dy = 0. \quad (9)$$

External forcing (wind stress) will be balanced by viscous dissipation, that is, by bottom and lateral friction. This flat bottom case results in unrealistically high friction coefficients if we want to have realistic zonal transport. A major modification introduced by inclusion of bottom topography is that the bottom form stress balances the forcing. This mechanism is inviscid and proves to be very effective in drastically reducing the total zonal transport compared to the flat bottom case. Indeed, the Bretherton theorem (9) in this case can be rewritten as (Ivchenko 1987; Vallis 2006):

$$\int_0^L (H_1 \overline{v_1' q_1'} + H_2 \overline{v_2' q_2'})\, dy = f_0 \int_0^L \overline{v_2 B}\, dy. \quad (10)$$

The term under the integral on the rhs of (10) is the topographic form stress since

$$f_0 \overline{v_2 B} = -\overline{p_2 \frac{\partial B}{\partial x}}, \quad (11)$$

where p_2 is the pressure in the lower layer.

In experiments with a flat bottom, there is no substantial variability in the zonal transport and no standing (stationary in time) eddies because of temporal and zonal invariance. The transient eddies can contain patterns propagating zonally but are independent (on average) of the zonal coordinate. A strong zonal mean jet forms in each layer with a maximum in the center when a sinusoidal distribution of zonal wind stress is applied (McWilliams et al. 1978; McWilliams and Chow 1981; Ivchenko 1984; Ivchenko et al. 1997; Olbers 2005; Ivchenko et al. 2008). The upper jet is stronger because the eddy-induced lateral Reynolds stress transfers the eastward momentum to its center making it narrower and more intense (Held 1975).

Experiments show that even a small zonal variation in B substantially reduces the zonal transport.

3. Numerical model and experiments with the eddy-resolving model

Progress in understanding eddy dynamics in zonal flows came after a number of studies used quasigeostrophic zonal channel models (McWilliams et al. 1978; McWilliams and Chow 1981; Wolff and Olbers 1989; Treguier and McWilliams 1990; Wolff et al. 1991; Ivchenko et al. 1997; Olbers 2005). Experiments were conducted with flows in rectangular channels of different zonal extent with or without topographic obstacles and driven by different wind stresses. The basic questions answered with QG models concern momentum balance, vertical penetration of momentum, and the convergence of zonal momentum in jets. The zonal channel represents a multiply-connected domain and needs auxiliary conditions, for which McWilliams (1977) conditions were used. The total zonal transport as well as the pattern of the mean flow and eddy activity proves to be strongly dependent on the presence, and details, of the bottom topography. Here we employ a slightly modified version of the quasigeostrophic model comprehensively described by Sinha and Richards (1999). The model geometry consists of a zonal reentrant channel of length L_x = 7680 km (sufficiently long to minimize upstream effects, the precise length is chosen for reasons of computational efficiency), width L = 1500 km and depth H = 5 km. Here, x, y and z axes are oriented eastward, northward, and vertically upward, respectively. The model solves the quasigeostrophic equations in Cartesian coordinates on a beta plane centered at 50°S. The flow is constrained by rigid boundaries to the north and south and is forced by a sinusoidal zonal eastward wind stress τ [$\tau_x = \tau_0 \sin(\pi y/L)$, $\tau_y = 0$, where τ_0 is a constant]. Dissipation is effected by a linear bottom friction law and a biharmonic lateral friction operator. The model is solved for two vertical normal modes, or equivalently, two vertical layers as these two formulations can be shown to correspond exactly (Flierl 1978). For the purposes of this paper we depart from Sinha and Richards (1999) and run the model in two-layer mode, adjusting the layer depths and reduced gravity to mimic the idealized Southern Ocean model of Wolff et al. (1991). We

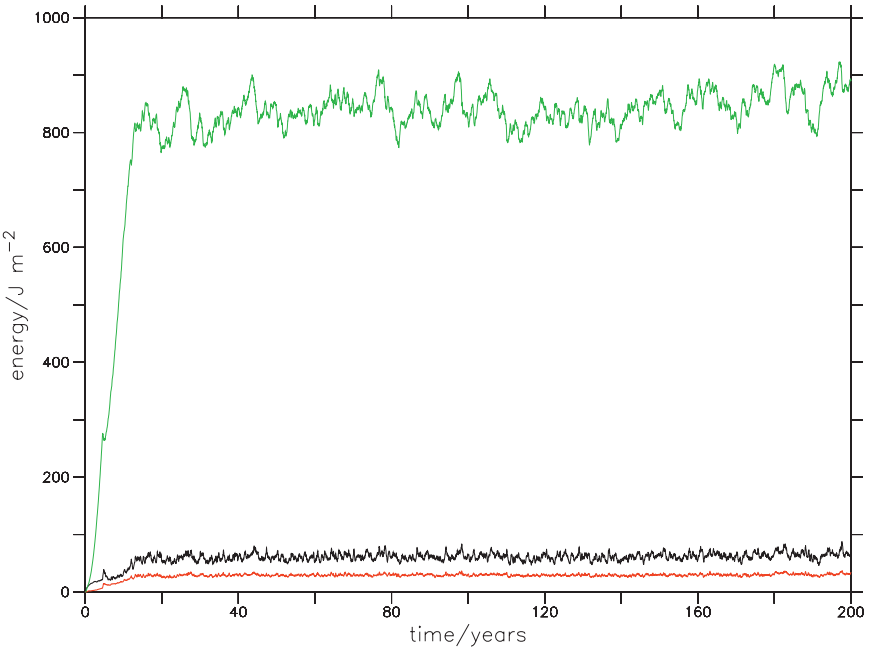

FIG. 1. Time series of kinetic energy (KE) for the upper layer (black), lower layer (red), and available potential energy (APE) (green) from the QG model.

also select a slightly finer grid resolution of 10 km and specify bottom topography, B that is sinusoidal in both x and y directions [$B = B_0 \sin(8\pi x/L_x) \sin(2\pi y/L)$] in order to correspond with the analytical solution derived in the following sections. Other than this, the model parameters are as listed by Sinha and Richards (1999) (Table 1 of their paper). In particular the Rossby radius, L_R, is set to be 36 km and the amplitude of the deviation of bottom topography $B_0 = 300$ m. The model is run from rest, forced by the specified constant (in time) wind stress for 200 model years and model statistics (mean layer wise streamfunction and potential vorticity) are obtained by averaging over the final 100 years of the experiment.

Numerical results

Figure 1 shows the domain-averaged layer wise kinetic energies and potential energy as a function of time. The model spins up to an equilibrated state within about 20 years and remains stable for the remainder of the experiment. Even after 200 years of integration, a small trend is discernible in the energy time series and small zonal and meridional asymmetries remain in the mean state (see subsequent figures). This suggests that an even longer integration is desirable; however, we do not expect any qualitative change in the solution after the initial (20 yr) adjustment phase. Instantaneous streamfunctions and potential vorticities at year 100 (Fig. 2) indicate that the model simulates narrow jets (compared with the forcing length scale) and a mature eddy field. Typical eddy length scales are of order 100–300 km and are well resolved by the model grid. The mean streamfunctions (Fig. 3) show two narrow jets (northern and southern), with meanders on the length scale of the sinusoidal topography. Importantly, the deflection over the topography is observed to be as predicted by the analytical solution. The zonal mean zonal velocity obtained from the derivative of the streamfunction is shown in Fig. 4. The two meandering jets show up as three regions of intense current. A zonal section of the mean streamfunction (Fig. 5) shows that the solution is dominated by the topographic length scale, but there are also clearly higher wavenumber harmonics present. This is illustrated in Fig. 6 which shows the Fourier spectrum of the mean streamfunction at the same latitude. The flow is almost entirely composed of wavenumbers 4, 6, and 8. We note that only wavenumber 4 will contribute to the topographic term in the generalized Bretherton relation (see Section 6) and that it is the dominant wavenumber in terms of amplitude. In fact for the form of topography specified, the topographic form stress will be determined solely by the wavenumber 4 component of the streamfunction, which is in phase with the topography.

As well as giving us an impression of the flow field associated with this configuration of bottom topography, the numerical results will be used later to estimate the free parameters of the analytical solution developed in the next sections.

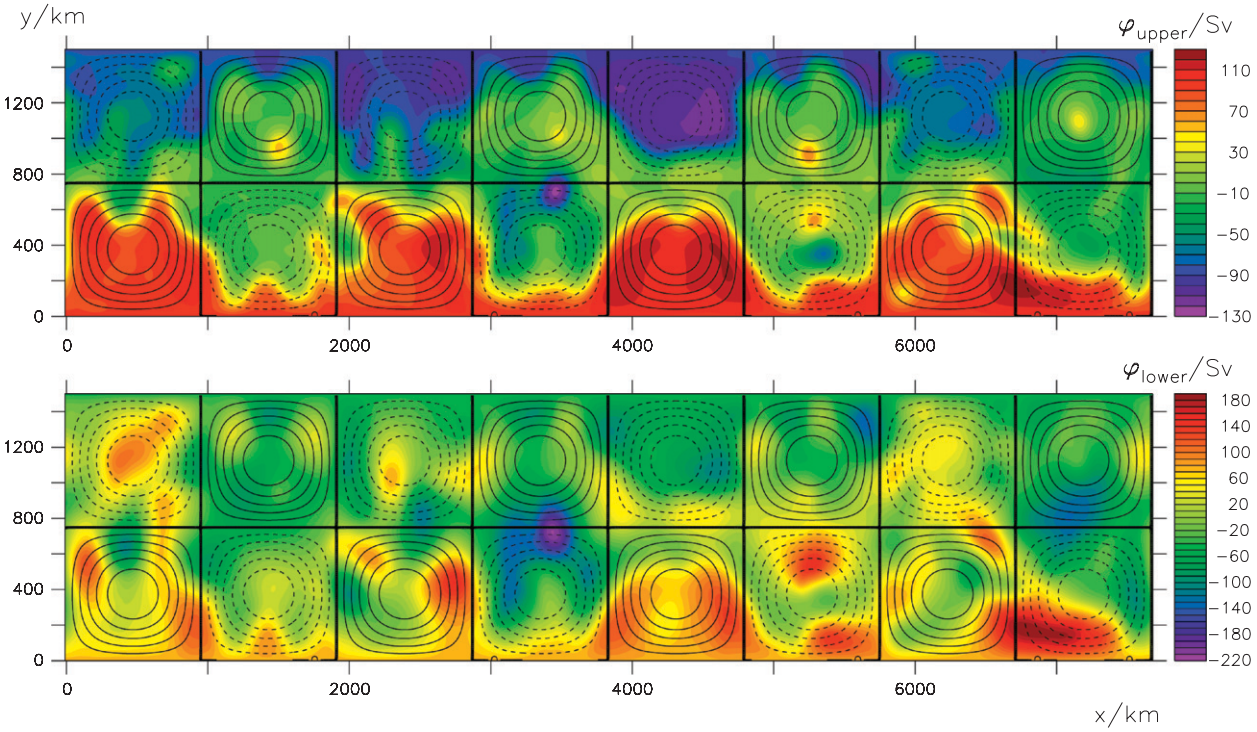

FIG. 2. Instantaneous (top) upper- and (bottom) lower-layer streamfunction (color shading) after 200 years of integration. Contours show the amplitude (max 300 m) of the bottom topography. Solid (dashed) contours indicated the positive (negative) topographic anomaly. Contour interval is 50 m.

4. Parameterization of eddy QPV fluxes

Let us assume a diffusive parameterization for QPV eddy fluxes. In the case of a 2-layer model this can be written as

$$\overline{v_i' q_i'} = -K_i \frac{\partial \overline{q}_i}{\partial y}, \tag{12}$$

where $K_i \geq 0$ is the coefficient of diffusion of quasi geostrophic potential vorticity (we will call it CPV).

Expression (10) places restrictions on the coefficients K_i. We set external forcing zonal wind stress τ_x to be sinusoidal in the meridional coordinate and independent of the zonal coordinate:

$$\tau_x = \tau_0 \sin\left(\frac{\pi y}{L}\right), \tag{13}$$

where τ_0 is an amplitude of zonal wind stress. We also set bottom topography deviation B as

$$B = B_0 \sin\left(\frac{2k\pi x}{L_x}\right) \sin\left(\frac{2\pi y}{L}\right), \tag{14}$$

where B_0 is the amplitude of bottom topography deviation. Such topography is periodic in the zonal direction, takes zero values at boundaries ($y = 0, L$), and has zero mean, $\overline{B} = 0$. We substitute (12) in the equations for QPV [(5)–(6)] for the steady state regime (i.e., neglecting time derivatives) and also neglecting the lateral friction, and rewrite them in nondimensional form (Marshall 1981; Ivchenko 1987; Ivchenko et al. 1997):

$$\gamma \frac{\partial}{\partial y^*}\left(\check{r}_1 \frac{\partial q_1^*}{\partial y^*}\right) - \frac{u_s}{u_c}\cos(\pi y^*) = 0, \quad \text{and} \tag{15}$$

$$\gamma \frac{\partial}{\partial y^*}\left(\check{r}_2 \frac{\partial q_2^*}{\partial y^*}\right) + \epsilon^* \frac{\partial u_2^*}{\partial y^*} = 0, \tag{16}$$

where the asterisk marks nondimensional parameters: $q_i = \beta L q_i^*$; $\gamma = L_R/L$; $L_R = (g' H_1 H_2/f_0^2 H)^{1/2}$; $y = Ly^*$; $\overline{u}_i = u_c u_i^*$; $\epsilon = \beta L \epsilon^*$; $\delta_i = H_i/H$; $\Psi_i = L u_c \Psi_i^*$.

The quantity $\check{r}_i$ is the nondimensional CPV, $\check{r}_1 = K_1/(L_R u_c)$, $\check{r}_2 = \Theta \check{r}_1$. We have $u_s = \pi\tau_0/H_1\beta L$; and $u_c = g'\beta H/f_0^2$; u_s is a typical wind-driven velocity; and u_c is a typical channel velocity, chosen with the expectation that vertical shears will build up sufficiently to balance the β-term in the expression for meridional gradient of QPV (Marshall 1981).

Expressions for meridional gradients of QPV are obtained by taking the time and zonal average of Eqs.

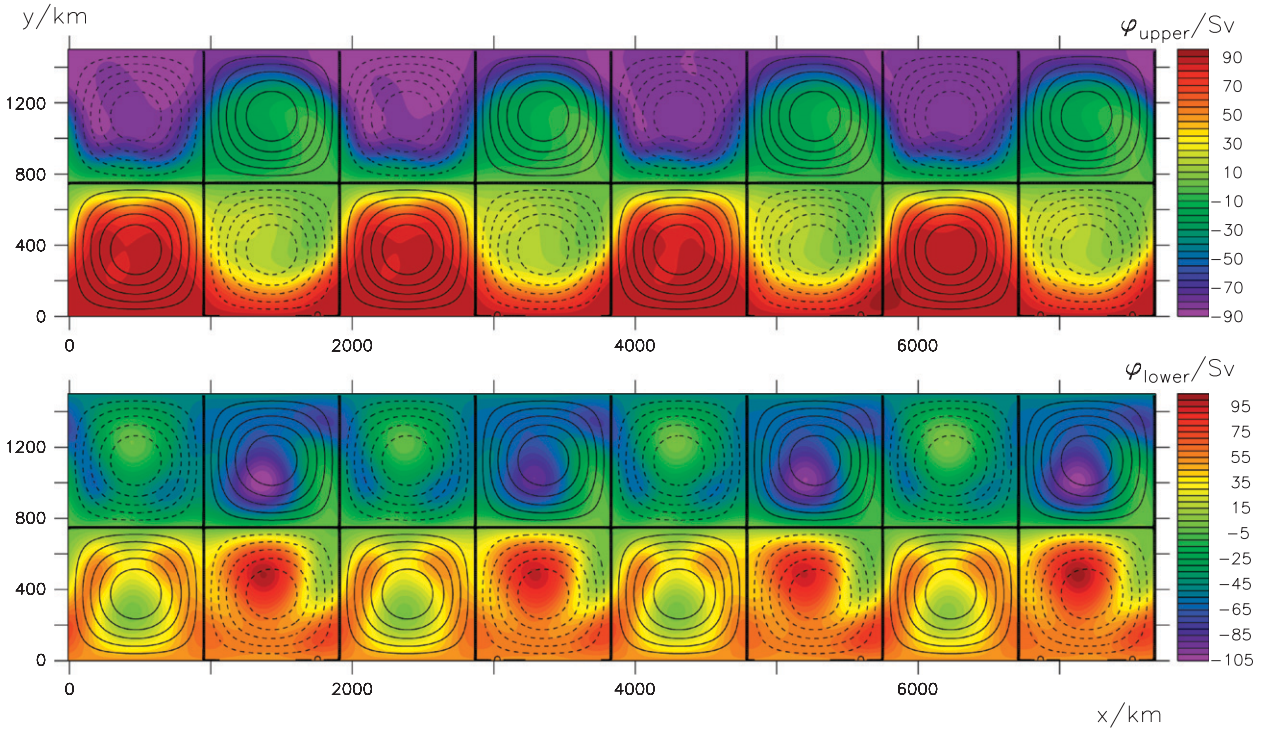

FIG. 3. As in Fig. 2, but for the mean streamfunction averaged over years 101–200.

(3)–(4) and then differentiating with respect to y. In nondimensional form these are

$$\frac{\partial q_1^*}{\partial y^*} = -\frac{\gamma^2}{\delta_1\delta_2}\frac{\partial^2 u_1^*}{\partial y^{*2}} + 1 + \frac{1}{\delta_1}(u_1^* - u_2^*), \quad \text{and} \quad (17)$$

$$\frac{\partial q_2^*}{\partial y^*} = -\frac{\gamma^2}{\delta_1\delta_2}\frac{\partial^2 u_2^*}{\partial y^{*2}} + 1 - \frac{1}{\delta_1}(u_1^* - u_2^*). \quad (18)$$

Further insight can be gained by solving analytically the system of Eqs. (15)–(18) for QPV for some arbitrary K_i profiles and then investigating the effect of the integral constraint (10).

The no-flux boundary condition at the walls should be satisfied, that is,

$$\overline{v_i' q_i'}|_{0,L} = 0, \quad (19)$$

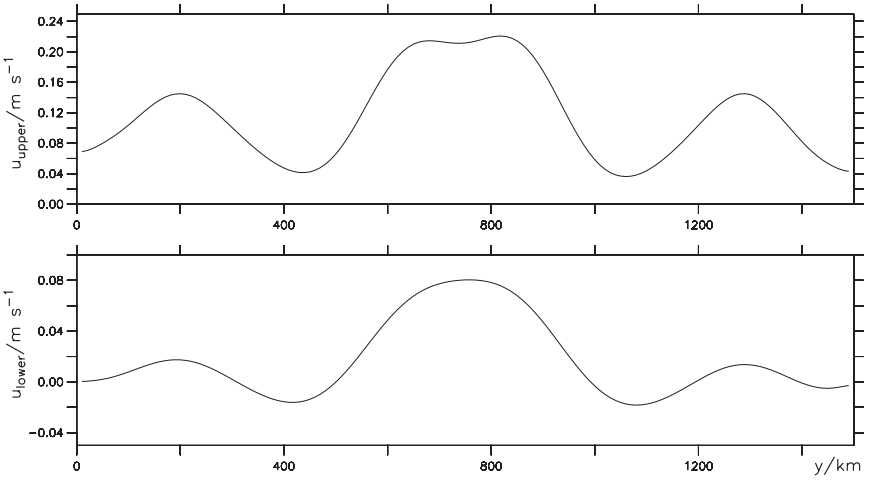

FIG. 4. (top) Upper- and (bottom) lower-layer zonal mean zonal velocity averaged over years 101–200.

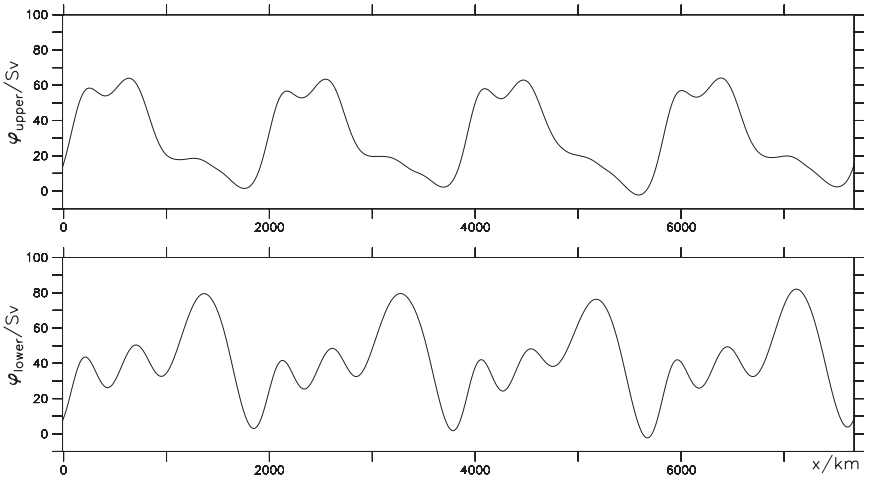

FIG. 5. (top) Upper and (bottom) lower time mean streamfunction as a function of zonal coordinate for $y = 600$ km, averaged over years 101–200.

or in nondimensional parameterized form, using (12):

$$\left(\check{r}_i \frac{\partial q_i^*}{\partial y^*}\right)\Big|_{0,1} = 0. \tag{20}$$

Coefficient $\check{r}_i$ (CPV) is a free parameter. As a first step we consider a constant value for the CPV in each layer and therefore their ratio $\Theta = \text{const}$. It would be worthwhile to consider a spatially variable CPV, for example, linked to u_i, q_i, and/or internal and external parameters, but it is not clear how one would proceed and to do so would prevent us from obtaining an analytical solution that provides important insight into the problem and enables us to find the minimal number of governing nondimensional parameters (for more detail see summary and discussion).

In the general case we cannot expect the meridional gradient of QPV to be zero on the walls. This means that CPV must be zero on walls. We consider steady flow in which the diffusivity for QPV in the main part of the current is constant almost everywhere, except small boundary layers near walls ($\Delta \ll 1$), where we assume the CPV to be proportional to the distance to the wall:

$$\check{r}_1 = \begin{cases} r = \text{const} & \Delta \le y^* \le 1 - \Delta \\ r \cdot y^* & 0 \le y^* \le \Delta \\ r(1 - y^*) & (1 - \Delta) \le y^* \le 1 \end{cases}. \tag{21}$$

The coefficient of diffusivity in the lower layer $\check{r}_2$ is $\check{r}_2 = \Theta \check{r}_1$ at any point, $0 \le y^* \le 1$. The Θ must be found from integral constraint (10).

We set streamfunctions Ψ_i and corresponding velocities in the form of a product of a meridionally varying function, $Q(y)$, and a zonally varying Fourier time series:

$$\Psi_i(x,y) = Q(y)\left[1 + \sum_{l=1}^{2N} a_l \sin\left(\frac{l\pi x}{L_x}\right) + \sum_{l=1}^{2N} b_l \cos\left(\frac{l\pi x}{L_x}\right)\right]. \tag{22}$$

To satisfy zonal periodicity (i.e., $\Psi_i|_0 = \Psi_i|_{L_x}$) the odd modes have to be excluded, that is,

$$\Psi_i(x,y) = \overline{\Psi_i}(y)\left[1 + \sum_{l=2}^{2N} a_l \sin\left(\frac{l\pi x}{L_x}\right) + \sum_{l=2}^{2N} b_l \cos\left(\frac{l\pi x}{L_x}\right)\right], \tag{23}$$

where l is constrained to be even. Note, that $Q(y)$ is equal to the zonal averaged value $\overline{\Psi_i}(y)$.

In the next section we will solve the time and zonally averaged Eqs. (15)–(16).

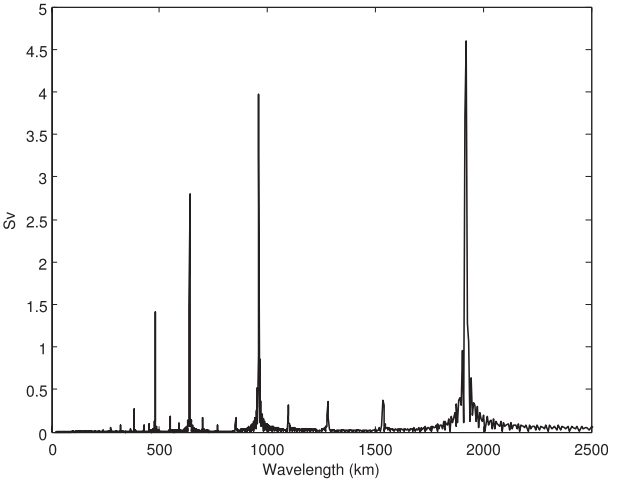

FIG. 6. Amplitude spectrum of the time mean (years 101–200) barotropic streamfunction for $y = 600$ km.

5. Zonally averaged solutions

Equations (15)–(16) for $\Delta \le y^* \le 1 - \Delta$ can be rewritten in the following form:

$$\frac{1}{\mathrm{Re}}\frac{d^2 q_1^*}{dy^{*2}} - \cos(\pi y^*) = 0, \quad \text{and} \tag{24}$$

$$\frac{1}{D}\frac{d^2 q_2^*}{dy^{*2}} + \frac{du_2^*}{dy^*} = 0, \tag{25}$$

where $\mathrm{Re} = u_s L/K_1$ is the analog of the Reynolds number, and characterizes the ratio of the forcing and QPV diffusion in the upper layer; $D = \epsilon u_c/(\beta K_2)$ characterizes the ratio of bottom friction to QPV diffusion in the lower layer.

Equation (24) represents the main dynamical balance in the upper layer, where the external forcing (curl of wind stress) is balanced by the eddy fluxes of the QPV. Equation (25) is the main dynamical balance for the lower layer, where the eddy fluxes of the QPV are balanced by bottom friction.

Equations similar to (24)–(25) can be written for the southern and northern boundary layers, that is, for the southern boundary, $0 \le y^* < \Delta$:

$$\frac{d}{dy^*}\left(y^*\frac{dq_1^*}{dy^*}\right) - \mathrm{Re}\Delta\cos(\pi y^*) = 0, \quad \text{and} \tag{26}$$

$$\frac{d}{dy^*}\left(y^*\frac{dq_2^*}{dy^*}\right) + D\Delta\frac{du_2^*}{dy^*} = 0. \tag{27}$$

Similar equations can be written for the boundary layer near the northern wall, that is, $1 - \Delta < y^* \le 1$ (not shown).

The system of equations is solved with boundary conditions that match QPV fluxes and velocities at the boundaries of the regions, that is, at $y^* = \Delta, 1 - \Delta$. As the forcing at the walls goes to zero, then

$$u_i^*|_{0,1} = 0 \tag{28}$$

(see Marshall 1981).

Our system has a small parameter γ, which characterizes the ratio of the Rossby deformation radius to the channel width. Substituting (17)–(18) into (24)–(27) one obtains a system of equations with a small parameter at highest derivative. Also in the equation for the lower layer there are regular singularities at the points $y^* = 0$ and $y^* = 1$. To solve the system we use an asymptotic expansion by a small parameter and to eliminate difficulties, related to the regular singularities we use a Frobenius method (Nayfeh 1973; Ivchenko et al. 1997), which is an asymptotic expansion in power series in the vicinity of regular singularities. We present u_i^* in the form of the following asymptotic series:

$$\begin{aligned} u_i^*(y^*) = {} & u_i^{(0)}(y^*) + \gamma u_i^{(1)}(y^*) + \gamma^2 u_i^{(2)}(y^*) + \cdots \\ & + \tilde{u}_i^{(0)}(\zeta) + \gamma\tilde{u}_i^{(1)}(\zeta) + \gamma^2\tilde{u}_i^{(2)}(\zeta) + \cdots \\ & + \tilde{\tilde{u}}_i^{(0)}(\xi) + \gamma\tilde{\tilde{u}}_i^{(1)}(\xi) + \gamma^2\tilde{\tilde{u}}_i^{(2)}(\xi) + \cdots . \end{aligned} \tag{29}$$

Here ζ and ξ are so-called "stretched coordinates," $\zeta = y^*/\gamma$, and $\xi = (1 - y^*)/\gamma$, $u_i^{(j)}(y^*)$ is a basic system of functions and $\tilde{u}_i^{(j)}(\zeta)$, and $\tilde{\tilde{u}}_i^{(j)}(\xi)$ are a system of "correction functions," which are important only near the walls and exponentially decreasing with distance, that is,

$$\tilde{u}_i^{(j)}(\zeta) \to 0, \quad as \quad \zeta \to \infty, \quad \text{and} \tag{30}$$

$$\tilde{\tilde{u}}_i^{(j)}(\xi) \to 0, \quad as \quad \xi \to \infty. \tag{31}$$

Solving our system we obtain the following asymptotic solutions for $\Delta \le y^* \le (1 - \Delta)$:

$$u_1^* = \left(\frac{\mathrm{Re}\delta_1}{\pi} + \frac{\mathrm{Re}\delta_1}{D\delta_2\pi}\right)\sin(\pi y^*) - \delta_1 - \frac{1}{D\delta_2} + O(\gamma^2), \quad \text{and} \tag{32}$$

$$u_2^* = \frac{\mathrm{Re}\delta_1}{D\delta_2\pi}\sin(\pi y^*) - \frac{1}{D\delta_2} + O(\gamma^2). \tag{33}$$

The asymptotic solutions for the thin boundary layer $0 \le y^* < \Delta$ can be written as

$$\begin{aligned} u_1^* = {} & (\mathrm{Re}\Delta\delta_1 - \delta_1)[1 - \exp(-\sqrt{\delta}_2\zeta)] \\ & + \frac{y^*}{D\Delta\delta_2}(\mathrm{Re}\Delta\delta_1 - 1) - \gamma\left[\frac{(\mathrm{Re}\Delta\delta_1 - \delta_1)}{4D\Delta\delta_2}\zeta\exp(-\sqrt{\delta}_2\zeta)\right] \\ & - \gamma\left[\frac{(\mathrm{Re}\Delta\delta_1 - \delta_1)}{4D\Delta\sqrt{\delta}_2}\zeta^2\exp(-\sqrt{\delta}_2\zeta)\right] + O(\gamma^2), \quad \text{and} \end{aligned} \tag{34}$$

$$\begin{aligned} u_2^* = {} & +\frac{y^*}{D\Delta\delta_2}(\mathrm{Re}\Delta\delta_1 - 1) \\ & - \gamma\frac{(\mathrm{Re}\Delta\delta_1 - \delta_1)}{D\Delta\delta_2}\zeta\exp(-\sqrt{\delta}_2\zeta) + O(\gamma^2). \end{aligned} \tag{35}$$

Similar solutions can easily be obtained for the other thin boundary layer $1 - \Delta < y^* \le 1$.

6. Integral constraint

Expression (10) can be written in dimensionless form as

$$\int_0^1 \left(\delta_1 r \frac{\partial q_1^*}{\partial y^*} + \delta_2 r\Theta \frac{\partial q_2^*}{\partial y^*}\right) dy^* = \frac{f_0 S}{HL_R u_c \beta} \int_0^1 \overline{v_2 B}^*\, dy^*, \tag{36}$$

where S is the scaling of $\overline{v_2 B}$, that is,

$$\overline{v_2 B} = S \times \overline{v_2 B}^*, \tag{37}$$

and v_2 is obtained from Ψ_2 in (23).

We have to split integrals over the main part of the channel (i.e., between $\Delta \le y^* \le 1 - \Delta$) and the two boundary layers ($0 \le y^* < \Delta$ and $1 - \Delta < y^* \le 1$):

$$\int_0^\Delta \left(\delta_1 r y^* \frac{\partial q_1^*}{\partial y^*} + \delta_2 r y^* \Theta \frac{\partial q_2^*}{\partial y^*}\right) dy^* + \int_\Delta^{1-\Delta} \left(\delta_1 r \frac{\partial q_1^*}{\partial y^*} + \delta_2 r\Theta \frac{\partial q_2^*}{\partial y^*}\right) dy^* + \int_{1-\Delta}^1 \left[\delta_1 r(1-y^*) \frac{\partial q_1^*}{\partial y^*} + \delta_2 r(1-y^*)\Theta \frac{\partial q_2^*}{\partial y^*}\right] dy^* = \frac{f_0 S}{HL_R u_c \beta} \left(\int_0^\Delta \overline{v_2 B}^*\, dy^* + \int_\Delta^{1-\Delta} \overline{v_2 B}^*\, dy^* + \int_{1-\Delta}^1 \overline{v_2 B}^*\, dy^*\right). \tag{38}$$

It is straightforward to calculate gradients of nondimensional QPV by using expressions for u_i^* for the main part of the channel [Eqs. (32)–(33) and for the southern [Eqs. (34)–(35)] and northern (not shown) boundary layers.

In our system there are two small parameters: $\gamma \ll 1$, and $\Delta \ll 1$. Substituting our asymptotic solutions for velocities and potential vorticities, it can be shown, that all contributions to the integrals in (38) from boundary layers can be disregarded, since they are of smaller order $O(\Delta^2)$, or $O(\Delta\gamma)$ or $O(\gamma^2)$ when compared with the contributions from the channel outside the boundary layers, $\Delta \le y^* \le 1 - \Delta$.

Note, that all ''sine'' components in (23) provide no contribution to the integral of bottom form stress [rhs of (36)]. The only nonzero contribution to the rhs of (36) from the ''cosine'' part of (23) is the component with the wavenumber equal to the zonal wavenumber of the topography, that is, where $l = 2k$.

The balance between the second integral in the lhs and the second integral of the rhs of (38) is

$$\frac{2\mathrm{Re}\delta_1}{\pi^2} r + r\Theta - r\Theta \frac{2\mathrm{Re}\delta_1}{\pi^2} = \frac{4 f_0 B_0 bk \delta_1 L^2 u_s \Theta}{3\pi HL_R L_x \delta_2 u_c \epsilon} - \frac{f_0 B_0 bkLr\Theta}{2HL_x \delta_2 \epsilon}, \tag{39}$$

where $b = b_{2k}$ in (23).

The lhs of expression (39) represents the integral of eddy fluxes of QPV, and the rhs is the topographic form stress. The ratio of eddy QPV diffusivity in the upper layer compared to the lower layer can be expressed in the following form:

$$1/\Theta = 1 + \frac{2B_0 L f_0 bk\pi}{3HL_x \delta_2 \epsilon} - \frac{\pi^2 L_R u_c r}{2\delta_1 u_s L} - \frac{B_0 \pi^2 L_R u_c f_0 bkr}{4\delta_1 u_s HL_x \delta_2 \epsilon}. \tag{40}$$

So, the ratio $1/\Theta$ is a function of nondimensional eddy QPV diffusivity in the upper layer and a number of parameters.

The expression (40) is our first constraint on the diffusivity coefficients. There are also two additional restrictions. One is based on the fact that topographic form stress can only decelerate the mean flow, that is,

$$f_0 \int_0^L \overline{v_2 B}\, dy < 0. \tag{41}$$

Another restriction is that coefficients in both layers should be positive or zero; zero values correspond to the trivial ''no-eddy'' regime and are not discussed. If both coefficients are positive then the rhs in (40) is positive.

Consider a channel in the Southern Hemisphere (''Southern Ocean''), $f_0 = -|f_0|$.

The wavenumber k in (40) is the zonal wavenumber of the bottom topography [see (14)]. In our numerical eddy-resolving experiments the value of k is equal to 4. For fitting–comparison of our theory with the numerical experiments we use the same value $k = 4$. We have calculated and plotted coefficient b as a function of latitude in Fig. 7. Values of b are predominantly negative, except small positive values near the lateral boundaries and spike in the center of the channel. The latter appears since the time- and zonal-mean streamfunction is close to zero at the center of the channel. The negative sign of b corresponds to conservation of QPV, that is, deflection of mean flow equatorward above a bump. The average value for the Fourier coefficient $b = -0.16$ (see Fig. 7). Let $b = -|b|$.

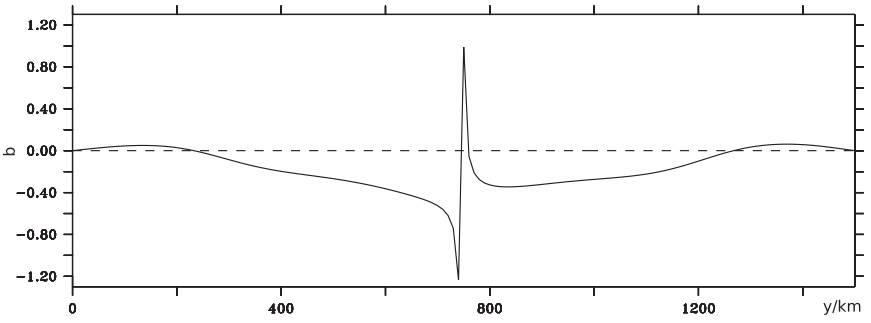

FIG. 7. Nondimensional amplitude of the wavenumber-4 component of the time mean lower layer streamfunction from the quasigeostrophic model (years 101–200). Only the amplitude of the component which contributes to the topographic form stress is included (see text for explanation).

Parameters α_T and α_B can be introduced as

$$\alpha_T = \frac{B_0 L |f_0||b|k}{H L_x \delta_2 \epsilon}, \quad \text{and} \tag{42}$$

$$\alpha_B = \frac{L_R u_c}{\delta_1 u_s L}. \tag{43}$$

The physical sense of parameter α_T is the relative importance of inviscid topographic form stress to viscous bottom friction. To discuss the physical sense of α_B we introduce two time scales: the first T_s is the time of propagation of particle with typical wind-induced velocity u_s over the distance of baroclinic Rossby radius L_R:

$$T_s = \frac{L_R}{u_s}. \tag{44}$$

Another time scale T_c is the time of propagation of a particle with the typical baroclinic velocity u_c over a distance corresponding to the channel width L:

$$T_c = \frac{L}{u_c}. \tag{45}$$

Parameter α_B is proportional to T_s/T_c, since

$$\alpha_B = \frac{L_R u_c}{\delta_1 u_s L} = \frac{H}{H_1}\left(\frac{L_R}{u_s}\right)\left(\frac{L}{u_c}\right)^{-1} = (H/H_1)\frac{T_s}{T_c}. \tag{46}$$

Equations (40) may be rewritten as

$$K_1/K_2 = \frac{1}{\Theta} = 1 + \frac{2\pi}{3}\alpha_T - \frac{\pi^2}{2}\alpha_B r - \frac{\pi^2}{4}\alpha_T \alpha_B r. \tag{47}$$

Expression (41) leads to the following restriction:

$$r < \frac{8}{3\pi\alpha_B}. \tag{48}$$

Because $K_1/K_2 > 0$, from (47), we have

$$r < R_{\text{cr}} = \frac{12 + 8\pi\alpha_T}{6\pi^2\alpha_B + 3\pi^2\alpha_T\alpha_B}. \tag{49}$$

Restriction (49) is stronger than (48).

Expression (47) together with (49) substantially restricts the values of the CPV.

In the flat bottom case $\Theta > 1$, that is, the coefficient in lower layer is higher than that in the upper layer (Marshall 1981), as can be seen from (47) with $\alpha_T = 0$ (since $B_0 = 0$):

$$K_1/K_2 = 1 - \frac{\pi^2}{2}\alpha_B r. \tag{50}$$

Since the rhs of (50) is less than 1 the CPV in the lower layer is higher than the CPV in the upper layer.

The condition that the $K_1 > K_2$ in the channel with bottom topography is

$$r < R = \frac{8\alpha_T}{6\pi\alpha_B + 3\pi\alpha_T\alpha_B}. \tag{51}$$

Note, that (51) is stronger than (49), that is,

$$R < R_{\text{cr}}. \tag{52}$$

With selected α_T and α_B the value of r cannot be greater than R_{cr}; approaching R_{cr} results in strong growth of CPV in the lower layer (see Figs. 8 and 9).

To estimate averaged values of α_T and α_B we used the output of our eddy-resolving experiment and external parameters from the model (see Sinha and Richards 1999). The mean values of the parameters α_T and α_B based on our eddy-resolving experiment are the following: $\alpha_T = 9.38$ and $\alpha_B = 0.85$.

If α_T is constant, increasing α_B leads to decreasing both R and R_{cr} (Fig. 8); If the time of propagation T_s of a particle with typical wind-induced velocity over the

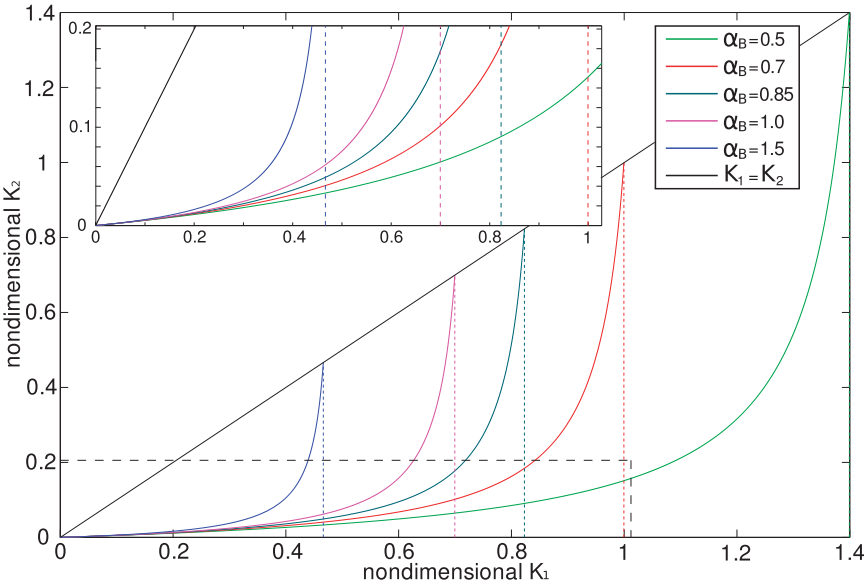

FIG. 8. Relationship between nondimensional upper (K_1) and lower (K_2) layer CPV as a function of α_B for fixed $\alpha_T = 9.38$ from the analytical solution [Eq. (47)] (colored solid lines). Colored dashed lines indicate the value of R [Eq. (51)]. The solid diagonal black line indicates $K_1 = K_2$. Inset shows an expanded portion of the main panel marked by the dotted black line.

distance of a Rossby radius is much greater than the time of propagation T_c of a particle with characteristic baroclinic velocity over the meridional channel width then (in limits) it tends to zero values of both $R_{\rm cr}$ and R: no eddying regime is permissible.

$$\lim_{\alpha_B\to\infty} R_{\rm cr} = 0, \quad \text{and} \tag{53}$$

$$\lim_{\alpha_B\to\infty} R = 0. \tag{54}$$

Conversely to the previous case, if α_B is very small, all values of $r < \infty$ are permissible and the coefficient in the upper layer is higher than that in lower layer.

$$\lim_{\alpha_B\to 0} R_{\rm cr} = \infty, \quad \text{and} \tag{55}$$

$$\lim_{\alpha_B\to 0} R = \infty. \tag{56}$$

In the case that α_B is constant, increasing the value of α_T leads to increasing values of $R_{\rm cr}$ and R (see Fig. 9), asymptotically approaching

$$\lim_{\alpha_T\to\infty} R_{\rm cr} = \frac{8}{3\pi\alpha_B}, \quad \text{and} \tag{57}$$

$$\lim_{\alpha_T\to\infty} R = \frac{8}{3\pi\alpha_B}. \tag{58}$$

Very high values of α_T correspond to dominance of inviscid topographic form stress, relative to viscous bottom friction. In this case both $R_{\rm cr}$ and R are finite and equal; the coefficient in the upper layer is higher than the in lower layer for any permissible r (see Figs. 8 and 9).

Very small values of α_T (dominance of viscous topographic friction over inviscid topographic form stress)

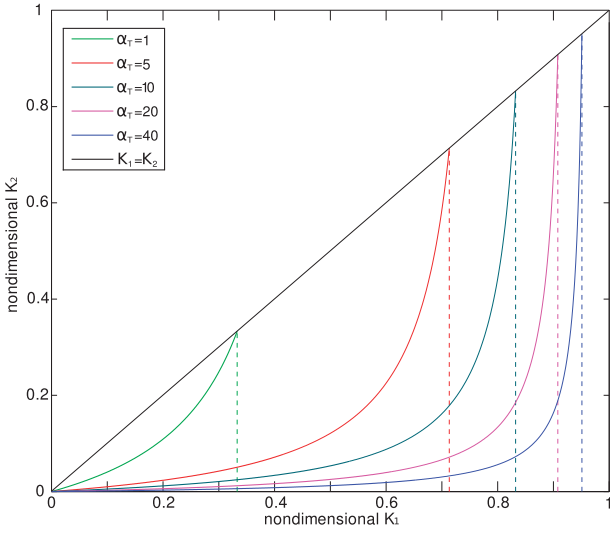

FIG. 9. Similar to Fig. 8, showing the relationship between upper (K_1) and lower (K_2) layer CPV as a function of α_T for fixed $\alpha_B = 0.85$.

leads to a finite value of $R_{\rm cr}$ which is inversely proportional to α_B:

$$\lim_{\alpha_T \to 0} R_{\rm cr} = \frac{2}{\pi^2 \alpha_B}, \tag{59}$$

In this case the coefficient in lower layer is greater than the coefficient in upper layer for all permissible r:

$$\lim_{\alpha_T \to 0} R = 0. \tag{60}$$

There is a caveat for extreme values of parameters α_B and α_T because quasigeostrophic scaling may be violated. However, it seems that the tendency of dependence of $R_{\rm cr}$ and R to extremes of these parameters makes physical sense.

7. Summary and discussion

New schemes for the parameterization of eddy fluxes in ocean models were developed in recent years (Eden 2010; Eden and Greatbatch 2008; Marshall et al. 2012; Marshall and Adcroft 2010; Ringler and Gent 2011). Indeed, we have to either resolve mesoscale eddies or parameterize them. In the latter case strict integral constraints must be satisfied. Note that not only ''internal values'' like mean PV, velocity and so on will be involved in such restrictions, but also geometry (bottom topography). We can a priori understand that for a diffusive parameterization of potential vorticity the inviscid term (topographic form stress) will be of leading order, since it participates in the main momentum balance: in the ACC topographic form stress balances wind stress input.

The CPV is a free parameter and cannot be negative both for physical and mathematical reasons. One can expect a complicated spatial distribution of this coefficient. Even in the simplest case with a flat bottom and sinusoidal meridional profile of wind stress (as used in this study), the CPV for the zonally averaged case has a ''double-bump'' distribution (see McWilliams and Chow 1981), that is, values increase from the boundaries to the periphery of the mean jet close to the center of the channel, and then reduce to a local minimum in the center of the channel, where the zonal velocity achieves the highest values. The physical hypothesis for the dependence of the CPV on variables of the model is important for realistic redistribution of momentum and QPV. However, such a relation is not yet known for channels with bottom topography. It is important to note that using a complicated expression for the CPV would allow us to obtain only a numerical solution and would prevent an analytical–asymptotic solution being obtained. Without an analytical solution we cannot find the integral constraint as an analytical function, like Eqs. (40) or (47) and an analytical function for physically meaningful parameters, like α_T and α_B. For this reason we use constant values of the CPV everywhere except for in the thin boundary layers. Our approach allows us to introduce two new parameters with a clear physical sense and this can provide advantages for application to more general cases (more complicated bottom topography, or even in closed basins): using these parameters will allow a simple and physically meaningful scheme of parameterization to be constructed.

We found a solution for the zonal channel with sinusoidally varying bottom topography both in meridional and zonal directions. The solution is an asymptotic expansion on the small parameter γ, which is the Rossby radius divided by the meridional size of the channel. The integral constraint, which is a generalized form of Bretherton's theorem, demonstrates the strong influence of bottom topography on the range of admissible values of the transfer coefficients. This approach could be used to find a solution to satisfy any smoothly varying bottom topography.

We have demonstrated that the CPV in the upper layer of the zonal channels with bottom topography must be higher than corresponding CPV in the lower layer [if the bottom topography deviation B is high enough, see (51)]. This is contrary to the flat bottom case.

The developed equation, based on integral constraint links effective values of CPV in upper and lower layers with two parameters: α_T and α_B. Parameter α_B is proportional to a time scale T_s, which is the typical time of propagation of the particle with a typical wind-induced velocity u_s over the distance of a baroclinic Rossby radius divided by time scale T_c, which is the time of propagation of the particle with typical baroclinic velocity u_c over a distance corresponding to the channel width L. The other important parameter α_T is the measure of importance of inviscid bottom form stress to the viscous bottom friction. The mean value of α_T was estimated directly from our eddy-resolving numerical model.

According to our theory the mean value of coefficient in the upper layer is a range between zero and $R_{\rm cr}$, [see Eq. (49)]. Expression (47) allows us to find a mean value for the coefficient in the lower layer for a given coefficient in the upper layer, r (or vice versa).

For the case of primitive equation models, eddy flux parameterizations must still satisfy a similar integral constraint if they are to produce physically correct results. This is particularly true for climate models, where it is necessary to trade resolution for faster computation,

and the use of such parameterizations is unavoidable. In contrast to parameterizations of eddy-induced tracer fluxes (such as the Gent–McWilliams scheme), which are both well established and fully incorporated into ocean general circulation models (and climate models), the effects of eddies on momentum are at present very crudely represented. The results presented here will be of relevance to the formulation of more sophisticated and accurate parameterizations schemes for eddy momentum fluxes in ocean general circulation models. In particular, analogous parameters to α_T and α_B and $R_{\rm cr}$ are likely to be of similar importance in more realistic models such as the NEMO ocean general circulation model (Madec 2008) and the HadGEM3 climate model (Hewitt et al. 2011).

Acknowledgments. We thank G.Reznik for his help with use of asymptotic expansions. We also thank two anonymous reviewers who provided a number of valuable comments, which allowed us to improve this study. Financial support was provided by the UK Natural Environment Research Council (Grant NE/H021396/1).

REFERENCES

Bretherton, F. S., 1966: Critical layer instability in baroclinic flows. *Quart. J. Roy. Meteor. Soc.,* **92,** 325–334.

Eden, C., 2010: Parameterising meso-scale eddy momentum fluxes based on potential vorticity mixing and a gauge term. *Ocean Modell.,* **32,** 58–71.

——, and R. J. Greatbatch, 2008: Towards a mesoscale eddy closure. *Ocean Modell.,* **20,** 223–239.

Flierl, G. R., 1978: Models of vertical structure and calibration of two-layer models. *Dyn. Atmos. Oceans,* **2,** 341–381.

Held, I. M., 1975: Momentum transport by quasi-geostrophic eddies. *J. Atmos. Sci.,* **32,** 1494–1497.

Hewitt, H. T., D. Copsey, I. D. Culverwell, C. M. Harris, R. S. R. Hill, A. B. Keen, A. J. McLaren, and E. C. Hunke, 2011: Design and implementation of the infrastructure of HadGEM3: The next-generation Met Office climate modelling system. *Geosci. Model Dev.,* **4,** 223–253.

Ivchenko, V. O., 1984: Parameterization of the eddy fluxes of the quasi-geostrophic potential vorticity in zonal flows. *Dokl. Acad. Nauk USSR,* **277,** 972–976.

——, 1987: The influence of bottom topography on the eddy transfer coefficient. *Izv. Akad. Nauk SSSR, Ser. Geofiz.,* **21,** 250–260.

——, K. J. Richards, and D. P. Stevens, 1996: The dynamics of the Antarctic Circumpolar Current. *J. Phys. Oceanogr.,* **26,** 753–774.

——, ——, B. Sinha, and J.-O. Wolff, 1997: Parameterization of mesoscale eddy fluxes in zonal ocean flows. *J. Mar. Res.,* **55,** 1127–1162.

——, S. Danilov, and D. Olbers, 2008: Eddies in numerical models of the Southern Ocean. *Ocean Modeling in an Eddying Regime, Geophys. Monogr.,* Vol. 177, Amer. Geophys. Union, 177–198.

Kamenkovich, V. M., M. N. Koshlyakov, and A. S. Monin, 1986: *Synoptic Eddies in the Ocean.* D. Reidel Publishing Company, 433 pp.

Madec, G., 2008: NEMO reference manual, ocean dynamic component: NEMO-OPA, Preliminary version. Institut Pierre Simon Laplace Note du Pole de Modelisation Tech. Rep. 27, 1288–1619.

Marshall, D. P., and A. J. Adcroft, 2010: Parameterization of ocean eddies: Potential vorticity mixing, energetics and Arnold's first stability theorem. *Ocean Modell.,* **32,** 188–204.

——, J. R. Maddison, and P. S. Berloff, 2012: A framework for parameterizing eddy potential vorticity fluxes. *J. Phys. Oceanogr.,* **42,** 539–557.

Marshall, J. C., 1981: On the parameterization of geostrophic eddies in the ocean. *J. Phys. Oceanogr.,* **11,** 257–271.

McWilliams, J. C., 1977: A note on a consistent quasigeostrophic model in a multiply connected domain. *Dyn. Atmos. Oceans,* **1,** 427–441.

——, and J. S. Chow, 1981: Equilibrium geostrophic turbulence. I. A reference solution in a beta plane channel. *J. Phys. Oceanogr.,* **11,** 921–949.

——, W. R. Holland, and J. S. Chow, 1978: A description of numerical Antarctic Circumpolar Currents. *Dyn. Atmos. Oceans,* **2,** 213–291.

Munk, W. H., and E. Palmén, 1951: Note on the dynamics of the Antarctic Circumpolar Current. *Tellus,* **3,** 53–55.

Nayfeh, A. H., 1973: *Perturbation Methods.* Wiley-Interscience, 437 pp.

Olbers, D., 2005: On the role of eddy mixing in the transport of zonal ocean currents. *Marine Turbulence. Theories, Observations, and Models,* H. Baumert, J. Simpson, and J. Sündermann, Eds., Cambridge University Press, 630 pp.

Pedlosky, J., 1979: *Geophysical Fluid Dynamics.* Springer Verlag, 624 pp.

Ringler, T., and P. Gent, 2011: An eddy closure for potential vorticity. *Ocean Modell.,* **39,** 125–134.

Scott, R. B., and F. Wang, 2005: Direct evidence of an oceanic inverse kinetic energy cascade from satellite altimetry. *J. Phys. Oceanogr.,* **35,** 1650–1666.

Sinha, B., and K. J. Richards, 1999: Jet structure and scaling in Southern Ocean models. *J. Phys. Oceanogr.,* **29,** 1143–1155.

Stevens, D. P., and V. O. Ivchenko, 1997: The zonal momentum balance in an eddy–resolving general–circulation model of the Southern Ocean. *Quart. J. Roy. Meteor. Soc.,* **123,** 929–951.

Treguier, A. M., and J. C. McWilliams, 1990: Topographic influences on wind–driven, stratified flow in a β–plane channel: an idealized model for the Antarctic Circumpolar Current. *J. Phys. Oceanogr.,* **20,** 321–343.

Vallis, G. K., 2006: *Atmospheric and Oceanic Fluid Dynamics. Fundamentals and Large-Scale Circulation.* Cambridge University Press, 770 pp.

Wolff, J.-O., and D. J. Olbers, 1989: The dynamical balance of the Antarctic Circumpolar Current studied with an eddy-resolving quasi-geostrophic model. *Mesoscale-Synoptic Coherent Structures in Geophysical Turbulence,* Elsevier, 435–458.

——, E. Maier–Reimer, and D. J. Olbers, 1991: Wind-driven flow over topography in a zonal β–plane channel: A quasigeostrophic model of the Antarctic Circumpolar Current. *J. Phys. Oceanogr.,* **21,** 236–264.